Journal of Materials Chemistry A



PAPER

View Article Online



Cite this: DOI: 10.1039/d1ta10867k

A flexible thin film lithium battery with a chemical vapor deposited organic complex cathode†

Zhuo Li, 🕩 Fei Hu, 🕩 Ni Huo 🕩 and Wyatt E. Tenhaeff 🕩

Organic cathode materials have attracted significant research attention recently, yet their low electronic conductivity limits their application as solid-state cathodes in lithium batteries. This work describes the development of a novel organic cathode chemistry with significant intrinsic electronic conductivity for solid-state thin film batteries. A polymeric charge transfer complex (CTC) cathode, poly(4-vinylpyridine)-iodine monochloride (P4VP·ICI), was prepared by initiated chemical vapor deposition (iCVD). Critical chemical, physical, and electrochemical properties of the CTC complex were characterized. The complex was found to have an electronic conductivity of 4×10^{-7} S cm⁻¹ and total conductivity of 2×10^{-6} S cm⁻¹ at room temperature, which allows the construction of a 2.7 μ m thick dense cathode. By fabricating a P4VP·ICI|LIPON|Li thin film battery, the discharge capacity of P4VP·ICI was demonstrated to be >320 mA h cm⁻³ on both rigid and flexible substrates. The flexible P4VP·ICI|LIPON|Li battery was prepared by simply replacing the rigid substrate with a flexible polyimide substrate and the as-prepared battery can be bent 180° while maintaining electrochemical performance.

Received 22nd December 2021 Accepted 3rd March 2022

DOI: 10.1039/d1ta10867k

rsc.li/materials-a

Introduction

Beyond their primary application in consumer electronics and electric vehicles, lithium-ion batteries (LIBs) are essential to advanced microelectronic applications such as smart cards, sensors, wearable electronics, and microelectromechanical systems (MEMs).1 These applications require miniaturized dimensions, mechanical flexibility, safety, and ease of packaging, in addition to good power performance and a long operational life. As solid-state energy storage devices, thin film batteries not only provide high intrinsic safety but also excel in many other key aspects, such as high volumetric energy density, fast charge/discharge rate and cyclability. The schematic provided in Fig. 1a shows the typical structure of a thin film battery. The fully dense film morphologies and lack of binder and conductive additives enable high volumetric energy, excluding the mass and volume of the substrate. The metal current collector, cathode, solid electrolyte and Li anode are deposited onto a substrate by a sequence of deposition processes, and the total thickness of the thin film battery is only several micrometers.2 For a typical thin-film battery with an intercalation cathode, a layer of amorphous material such as LiCoO2 (LCO) or LiMn2O4 (LMO) is deposited onto a metalized substrate by radiofrequency (RF) sputtering and then annealed to crystallize into the optimal crystalline

microstrcuture.^{3,4} Subsequently, a solid state electrolyte, lithium phosphorus oxynitride (LIPON), is deposited directly onto the cathode. Its decent lithium ion conductivity (10⁻⁶ S cm⁻¹), extremely low electronic conductivity (on the order of 10⁻¹⁴ S cm⁻¹), wide electrochemical stability, and large elastic modulus enable stable cycling of Li metal anodes.^{5,6} Finally, Li metal is evaporated onto the solid electrode layer to create the anode. Thin film batteries are a prime example of highly reversible charge/discharge in solid-state Li metal batteries.²

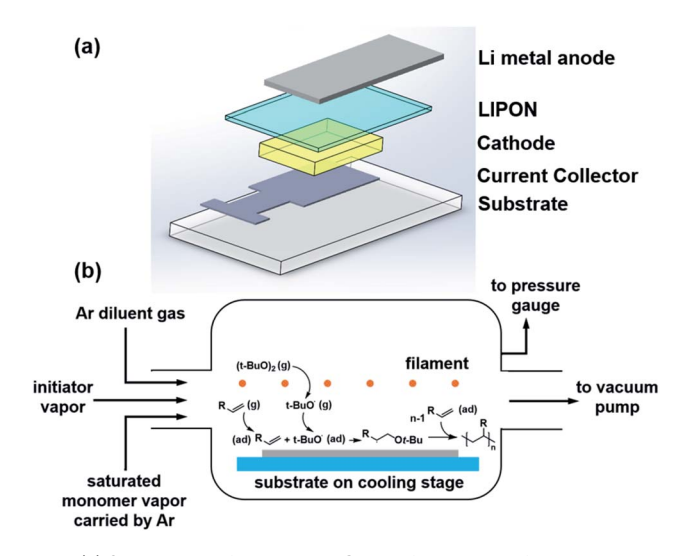


Fig. 1 (a) Schematic of the P4VP-ICI thin film battery fabricated in this study. (b) Schematic illustration of the iCVD reactor and reactions.

Department of Chemical Engineering, University of Rochester, Rochester, New York 14627, USA. E-mail: wyatt.tenhaeff@rochester.edu

† Electronic supplementary information (ESI) available. See DOI: 10.1039/d1ta10867k

However, a thin film battery with an intercalation cathode is still limited in several important factors, especially processing speed and scalability. First, deposition of both the cathode and the electrolyte material is most frequently performed by RF sputtering.4 The deposition rate of dielectrics by RF sputtering is considerably slower than for conductive materials. ⁷ Since the thickness of practical thin film batteries is usually several micrometers, the throughput of RF sputtering is a significant limitation. Second, the utilization of intercalation cathodes constrains the substrate composition since high temperature annealing is required to generate the desired microstructure. Typical substrates include alumina, quartz, and silicon wafers. This high temperature thermal annealing excludes most flexible thermoplastic materials as potential low-cost alternative substrates. An indirect approach for preparing flexible thin film batteries has been demonstrated by Koo et al., where the cell is first deposited on mica and transferred to PDMS which is a flexible support.8 While the electrochemical performance is preserved, the processing is very delicate and not readily scaledup. Finally, recrystallization of the sputtered electrolyte results in microstructural orientation (texturing) due to thermal stress, which also leads to rough surface topographies and film fracture.9 Compensating for the increased surface roughness and defects requires a thicker solid electrolyte layer (LIPON), which further reduces the throughput by increasing the required deposition duration.

To address these intrinsic challenges associated with intercalation cathodes, novel cathode chemistries are needed with comparable energy storage performance. Solid, amorphous thin film cathodes are expected to significantly increase processing throughput, reduce cost, and enable flexible polymeric substrates by eliminating the thermal annealing step. Many novel cathode chemistries have been developed for solid state batteries, such as organic and conversion type cathodes (halogen, halide, sulfur etc.). 10,11 Among them, organic cathodes are attractive due to their sustainability and considerable cost advantage over intercalation materials. 12,13 When cast as a composite cathode (consisting of an organic active material, conductive additive, and polymeric binder) and employed in a conventional lithium ion cell with a liquid electrolyte, organic cathodes can deliver high specific capacity/energy and acceptable cyclability.¹³ Yet solid-state organic batteries are limited by the very low electronic conductivity of the organic active material. In conventional lithium ion cells, the problem is circumvented by adding large amounts of conductive additive (>30%) to the composite cathode. 12,13 In dense, solid-state electrolytes without additional conductive additive, it was found that approximately only the first 10 nm of the cathode layer is electrochemically active, regardless of the deposited thickness.14 By comparison, thin film cathodes are usually >1 µm thick; ideally, they are deposited as thick as possible since the cathode volume defines the overall energy density of the cell.15 To achieve comparable areal specific capacity with layered oxide thin film batteries, the electronic conductivity of the organic cathode must be increased.

This work is aimed at providing a possible solution to these challenges by constructing a thin-film system with a novel

organic cathode material. Two objectives are expected to be achieved in the work: (1) identify an amorphous solid cathode material that allows non-PVD deposition to increase the throughput of cathode preparation and allow wider processing capabilities and (2) reduce the required thickness of the LIPON electrolyte by introducing an isotropic, amorphous cathode, which further lowers the manufacturing time and cost. Initiated chemical vapor deposition (iCVD) was chosen as a fast deposition method. Among various methods of depositing organic polymeric films, iCVD has several important advantages, such as high deposition rates, broad compositional versatility and tunability, deposition conformality and processing simplicity.16 A schematic of iCVD used in this work is shown in Fig. 1b. During the iCVD process, the initiator vapor passes over a heated filament, generating gas-phase radicals. Monomer vapor and initiator radicals are then adsorbed onto the substrate and polymerize on the surface. Since the polymerization proceeds in the adsorbed phase, deposition of the polymer is conformal.17 In comparison, RF sputtering is slow and typically line-of-sight, often resulting in non-conformal deposition on the substrate. In this work, a dense and smooth polymer film was prepared by iCVD on a current collector as the matrix for the electrochemically active species.

A novel strategy utilizing a charge transfer complex (CTC) between a halogen and basic polymer matrix was examined to solve the issue of low electronic conductivity. The CTC between a halogen/amine is known as a mixed ionic-electronic conductor (MIEC) with considerable electronic/ionic conductivity. Both the solution and neat CTC between halogen/interhalogen and pyridine are ionically and electronically conductive. 18,19 In addition, previous studies on Li–halide batteries guide the development of halogen-based CTC batteries. For example, with an appropriate absorbent such as poly(vinylpyrrolidone) or carbon, $\rm I_2$ can deliver a voltage of >2.7 V and a capacity of >200 mA h g $^{-1}$ in an aqueous or organic liquid electrolyte. $^{20-22}$ A solid-state lithium– $\rm I_2$ battery with an $\rm I^-$ conductor has also been previously demonstrated. 23

In this work, a complex of poly(4-vinyl pyridine) (P4VP) and iodine monochloride (ICl) was thoroughly explored as a CTC cathode. The polymer matrix is chosen because pyridine has relatively high basicity among organic bases (p $K_a = 5.2$ of conjugate acid), which allows the formation of a stable CTC with a halogen/interhalogen,²⁴ and the iCVD of P4VP is an established method allowing fast and reproducible preparation of the CTC cathode.²⁵ ICl was chosen as the electrochemically active reagent in the CTC due to its high voltage (>3.6 V, demonstrated in this work) and high theoretical specific capacity (330 mA h g⁻¹). These properties make P4VP·ICl a favorable cathode material compared to Li/I₂ (2.7 V) and Li/Br₂ (3.4 V).^{23,26} In addition, the higher Lewis acidity of ICl leads to a more stable charge transfer compound with P4VP, enabling the subsequent vacuum deposition of LIPON.

This study describes the development of P4VP·ICl for thin film batteries. A thin film P4VP·ICl complex was prepared, and its essential properties were characterized and then compared to those of P4VP·I₂. Flexibility of the battery was achieved by replacing the quartz substrate with Kapton, a widely used

polyimide material. The cyclability of the P4VP·ICl system was also examined and future work with novel polymer matrices with higher oxidative stability, lower α-H activity and higher basicity is proposed.

Experimental methods

Preparation of CTCs

Two CTCs, P4VP·ICl and P4VP·I₂, were prepared in bulk and as thin films. To prepare P4VP·ICl in bulk, 1 g P4VP (Scientific Polymer Products, viscosity average molecular weight = 200 000 g mol⁻¹) was dissolved in 150 mL 2-propanol (Fisher Scientific, 99%) to form a colorless solution. Then, 1.60 g ICl (1.04 eq.) was dissolved in 100 mL THF (Fisher, HPLC grade), forming a red to brown solution. Be advised that the solvation of ICl in THF is highly exothermic and may splatter. The ICl solution was added dropwise into strongly agitated P4VP solution, and light-yellow precipitate formed immediately. After adding the ICl solution, the reaction mixture was rested for 30 min. The precipitate was filtered and washed with isopropanol until the wash was colorless. The precipitate was then vacuum dried for 2 h at room temperature and stored in a desiccator. The product, P4VP·ICl is a slightly yellow powder, obtained in near theoretical yield. P4VP·I2 is prepared with a similar method, replacing ICl with I₂ (2.52 g, 1.04 eq.). Both P4VP·ICl and P4VP·I2 are insoluble in THF, isopropanol, diethyl ether and dimethyl carbonate, soluble in DMF and DMSO, and react with acetone.

To prepare P4VP·ICl and P4VP·I2 as thin film cathodes, a P4VP thin film is first deposited onto a Pt current collector. A 70 nm thick platinum layer was sputtered onto a quartz substrate (1 \times 1 \times 0.04 inch) using DC sputtering. For flexible thin film batteries, the quartz substrate is replaced with Pt metalized Kapton® film (McMaster-Carr, 0.05 mm thickness). The P4VP thin film was then deposited on the Pt using iCVD to fully cover the current collector area, while a small section on the edge of the substrate was masked during deposition to allow electrical contact. The effective battery area was 0.6 cm² $(0.4 \times 1.5 \text{ cm})$, defined by the area of the Pt current collector pad coated with P4VP. A schematic illustration of the battery fabrication process and the definition of the active area can be found in Fig. S1.† P4VP was prepared using a custom built iCVD system employing argon carrier gas. A flow of high purity argon (5 sccm) was used to introduce 4-vinylpyridine (Fisher, 95% pure, kept at 25 °C) vapor into the chamber. 2 sccm di-tert-butyl peroxide (TBPO, Fisher, 99% pure) was used as the initiator. Additional 10 sccm argon patch flow was used to dilute the precursor feed to provide better film uniformity.27 The quartz substrate was placed on a copper stage kept at 25 °C using a liquid temperature control chiller. The chamber pressure was regulated at 1000 mTorr. The thickness of the deposited film was monitored in situ with a laser interferometer. Typically, 1.6 µm thick poly(4-vinylpyridine) was deposited onto the substrate over 100 min. The deposited P4VP thin film was kept in a desiccator overnight to prevent physical adsorption of moisture before halogen incorporation.

After deposition of the P4VP film, I2 or ICl is incorporated into the P4VP thin film. For P4VP·I2, I2 was incorporated into the P4VP film using solution treatment. The film is immersed in 0.08 mol L⁻¹ I₂-hexanes solution overnight in an argon filled glovebox (I₂: Sigma-Aldrich, >99.99% purity; hexanes: Optima, HPLC grade). After the treatment, the film is washed with neat hexanes until no I2 color is seen in the wash. For P4VP·ICl, ICl was incorporated into the P4VP film using gas phase treatment due to the low solubility of ICl in hexanes. Red lighting is essential for this step, as ICl is highly photosensitive. A common fluorescent lamp causes heterolysis of ICl and degradation of the P4VP film over a long period of treatment. A drop of ICl liquid is placed in a small open glass container and is sealed with the P4VP sample inside a larger glass jar. The jar is left in an incubator set to 30 °C for 1 h. A saturated ICl gas atmosphere is created inside the jar and ICl absorption into the polymer film was observed.

Characterization of CTCs

To determine the stoichiometry and vacuum resistance of P4VP·ICl and P4VP·I₂, 2 μm thick P4VP was deposited on a preweighed Si wafer. The P4VP coated wafer was heated at 70 °C overnight to remove physically adsorbed monomers. The sample is weighed again with a Mettler Toledo XPR6UD5 microbalance (0.5 µg accuracy). Then, ICl and I2 were incorporated into the film. The CTC samples were kept in a desiccator for 24 h to remove any physically adsorbed halogen before weighing again. The weighed samples were then moved to a vacuum desiccator and pumped down for 30 min. The samples were weighed again to measure the vacuum loss of halogen. The optical properties and thicknesses of the P4VP·ICl films were characterized using a J. A. Wollam RC2 ellipsometer. Ellipsometric data were collected at an incident angle of 65° over the wavelength range of 210-1690 nm. Cauchy and Basis spline (B-spline) models were used to fit the transparent and absorbing regions of P4VP·ICl thin films, respectively. The refractive index dispersion spectrum of each layer was derived by fitting the experimental data with the calculated model data. To confirm the structure of P4VP·ICl and P4VP·I₂, UV-Vis and FTIR spectra were collected. For UV-Vis (ThermoScientific evolution 300), 50 nm thick P4VP was coated on a quartz substrate, and ICl/I2 was incorporated into the film. The spectrum was collected with 1 nm interval from 190 nm to 800 nm. For the FTIR spectrum, 2000 nm thick films of P4VP, P4VP·ICl and P4VP·I2 were coated onto an IR transparent Si wafer. The spectrum was collected with a Thermo Scientific Nicolet iS-50 infrared spectrometer with 4 cm⁻¹ resolution, integrated over 32 scans. The bare Si spectrum is subtracted from the data to obtain the spectrum of the complexes. White light interferometry (Zygo NewView 600) was performed on the P4VP film to confirm the surface roughness of the P4VP film.

Electrochemistry

To characterize the energy storage performance of P4VP·ICl, thin-film batteries consisting of P4VP·ICl|LIPON|Li were prepared by RF sputtering and Li evaporation. First, 150 nm LIPON is sputtered onto the cathode using radiofrequency sputtering. A Li₃PO₄ target (99.9%, Kurt J. Lesker) is sputtered under an ultrahigh purity N₂ atmosphere (20 mTorr) using an RF sputtering system (80 W plasma power) with 75 nm h⁻¹ deposition rate. The cathode–electrolyte stack is transferred into an argon filled glovebox (H₂O < 10 ppm) and a 1.5 μ m thick Li metal anode is thermally evaporated onto the LIPON surface.

Cyclic voltammetry of P4VP·ICl was performed on a P4VP·ICl|LIPON|Li cell at 70 °C with 0.5 mV s $^{-1}$ scanning rate. The cell is scanned between 3.7 V and 2.0 V. For charge/discharge experiments, the P4VP·ICl|LIPON|Li thin film battery was kept under an argon atmosphere (H2O and O2 < 1 ppm) during testing. The cell is clamped onto a custom designed battery holder, which is thermostatted during testing. The cell was discharged from the OCV to 2.0 V at various temperatures (37 °C, 55 °C, and 70 °C) and current densities (5 $\mu A~cm^{-2}$, 10 $\mu A~cm^{-2}$ and 20 $\mu A~cm^{-2}$). For characterization of reversibility, the cell is recharged at 10 $\mu A~cm^{-2}$ to 3.7 V and held at 3.7 V until the residual current is below 0.1 μA . A Biologic SP-300 potentiostat was used for electrochemical measurements.

Results and discussion

Physical properties of P4VP·ICl and P4VP·I $_2$ charge transfer complexes

A custom iCVD chamber was employed for the deposition of P4VP films. The overall process is described in Scheme 1. The vapor-phase reaction mixture is introduced into a pressure-controlled deposition chamber and passed over a heated nichrome filament suspended above the substrate. Radical species are generated by the thermal decomposition of TBPO. Monomers and initiator radicals are adsorbed onto the temperature-controlled substrate, and radical polymerization

radical generation: $(t-BuO)_2(g)$ $\xrightarrow{Ni-Cr}$ $\xrightarrow{filament}$ 2 t-BuO (g)adsorption: (g) \xrightarrow{Pt} substrate $\xrightarrow{298K}$ (ad)initiation: (ad) + t-BuO (ad)to (ad) + t-BuO (ad)termination: (ad) + (ad)

Scheme 1 Reactions in the iCVD process. Multiple termination routes are possible: radical recombination is shown as an example.

occurs subsequently on the substrate surface to form a conformal P4VP coating. 16,25

The iCVD method provides a fast deposition rate on the order of 15 to 20 nm min⁻¹ for P4VP, and the prepared film was utilized for CTC formation without additional post-processing. While the deposition rate of iCVD polymers can easily reach 100 nm min⁻¹ or greater, the deposition rate was deliberately limited in this study to ensure good thickness uniformity on the battery current collectors.16 On the other hand, sputtering of intercalation materials, such as LCO, is typically much slower (deposition rate <10 nm min⁻¹) and requires thermal annealing to crystallize into a polycrystalline microstructure.28,29 The surface roughness of the P4VP film was confirmed with white light interferometry (Fig. S2†). The film is smooth with a root mean square roughness of 1.1 nm. In comparison, surface texture and cracks often develop in annealed intercalation cathodes due to the thermal stress from annealing.9 Thicker electrolyte layers are required to compensate for this roughness and fully cover the layer and prevent shorting. Given its smooth surface topography, P4VP-based cathodes should allow for thinner electrolyte layers and hence, lower electrolyte resistances.

To prepare the cathode material, the P4VP film is further treated with halogen compounds to form charge transfer complexes. Two materials, P4VP·I2 and P4VP·ICl were prepared. I₂ was incorporated into the P4VP film by immersing the film in 0.08 M I₂-hexanes solution. Due to the larger polarity of the ICl molecule, ICl has limited solubility in nonpolar hexanes; thus, gas phase incorporation was employed to prepare P4VP·ICl instead. This was achieved by simply exposing the film to saturated ICl vapor in a sealed vessel. The ICl incorporation resulted in a 154.7 \pm 7.5% increase in mass from that of the initial P4VP film, suggesting that a 1:1 complex between ICl and the pyridine ring formed (expected increase for a 1: 1 complex $[C_7H_7N \cdot ICl]$ is 154.4%). For P4VP·I₂, the mass of the precursor P4VP film increased by 237.3 \pm 20.7% upon I_2 incorporation, which is also close to the expectation for a 1:1 complex $[C_7H_7N \cdot I_2]$ (241.4%).

Digital photographs and UV-Vis spectra of the complex films are provided in Fig. S3.† The precursor P4VP film has negligible absorption in the visible range and appears colorless and transparent. P4VP·I₂ strongly absorbs UV light ($\lambda_{peak,1} = 251$ nm) and blue light ($\lambda_{peak,2} = 389$ nm), thus appearing dark brown to red in color. P4VP·ICl has strong, complex absorption in the UV region (220-246 nm) but only weak absorption in the visible range (>380 nm), and thus appears to be slightly yellow. The color difference between P4VP·ICl and P4VP·I $_2$ can be explained by the polarity of the CTC compound. Interaction between iodine and an electron donor is known to cause a strong blue shift of the I2 absorption peak, and thus the brown to red color of P4VP·I₂ is caused by the Py–I $^{\delta+}$ –I $^{\delta-}$ polarization. 30,31 Due to the much larger electronegativity of Cl, P4VP·ICl is more ionic, which further blue-shifts the absorbance of P4VP·ICl into the UV range, explaining its limited color and transparency in the visible region.32

To further understand the structure and interactions between I_2/ICl and P4VP, FTIR spectroscopy of P4VP, P4VP· I_2

and P4VP·ICl was executed (Fig. 2). Vibrational modes of I-Cl and polarized I-I bonds are found in the far infrared region (<400 cm⁻¹) and cannot be resolved within the mid-IR optics of the FTIR spectrometer.33 Yet the interaction between I2/ICl and the pyridine ring can still be detected by the change in pyridine ring vibrational modes (650–1700 cm⁻¹). Key vibrational modes are summarized in Table 1.34

IR spectra of P4VP and P4VP·I₂ are in good agreement with a previous report, which confirms the formation of the P4VP·I₂ complex.35 A consistent trend of peak shifting can be observed in both P4VP·ICl and P4VP·I2, caused by the electron redistribution to the $I^{\delta+}$ center in CTCs. P4VP·ICl has a larger impact on both intensity change and peak shifting than P4VP·I₂. The intensity of free pyridine ring vibration (mode 8b, 1556 cm⁻¹) decreases in both P4VP·I₂ and P4VP·ICl, nearly disappearing in the latter spectrum. As a stronger Lewis acid, ICl causes stronger electron redistribution from N in the pyridine ring to the $I^{\delta+}$ center than I_2 , which causes the pyridine ring to have a lower electron density than in P4VP·I2. Hence, the shift of the pyridine ring vibrational modes is more significant in P4VP·ICl.36 Another notable change in Fig. 2a is the splitting of mode 8a. The 1597 cm⁻¹ P4VP 8a mode becomes two peaks, which correspond to the CTC and protonated pyridinium ring.37 In P4VP·ICl, the 1597 cm⁻¹ peak splits to 1610 cm⁻¹ (R-Py·ICl) and 1637 cm⁻¹ (pyridinium). In P4VP·I₂, the 1597 cm⁻¹ peak splits to 1607 cm⁻¹ (R-Py·I₂) and 1632 cm⁻¹ (pyridinium), while the relative intensity of the pyridinium peak is significantly lower than in the corresponding P4VP·ICl. The higher wavenumber pyridinium peak suggests two important facts: (1) hydrogen halide species are generated during the incorporation and (2) hydrogen halide formation during the ICl incorporation is much more prominent. Evidence of the formation of protonated pyridinium is also found in the 2700-3350 cm⁻¹ region (Fig. 2b). Most of the peaks remain unchanged in P4VP and CTCs, yet three strong new peaks are found in the P4VP·ICl complex. The additional peaks (>3067 cm⁻¹) are in agreement with the FTIR spectrum of Py·HCl, and correspond to the pyridinium N⁺-H vibration modes.³⁷⁻³⁹ Formation of hydrogen halides in the pyridine-halogen system via α-H substitution has been reported before, and is explained in Scheme 2.40

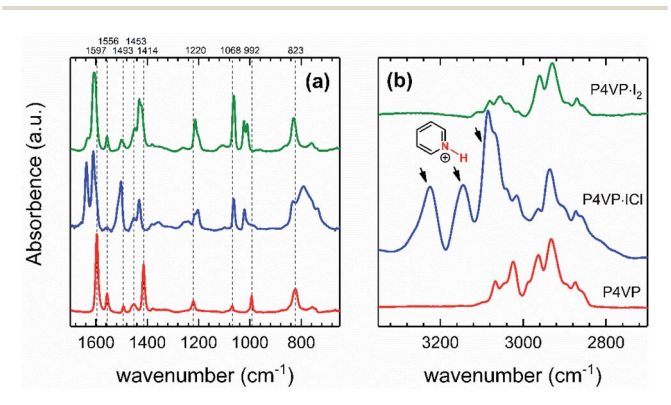


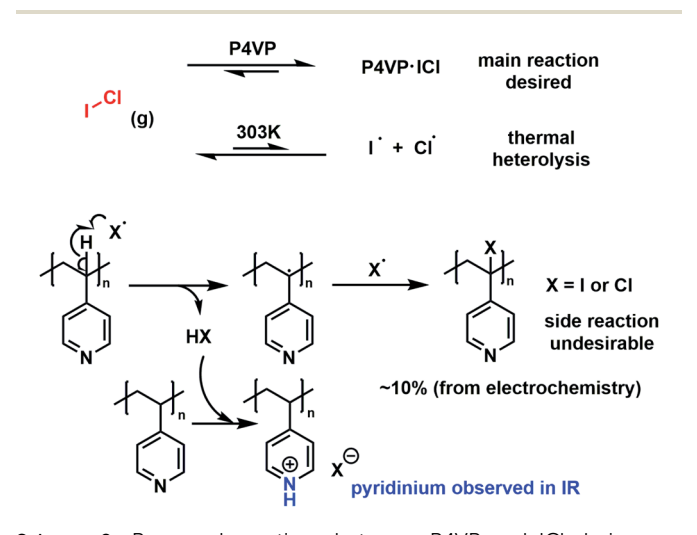
Fig. 2 FTIR spectra of P4VP and its CTC complexes: (a) 1700 cm⁻¹ to 650 cm^{-1} , (b) 3350 cm^{-1} to 2700 cm^{-1}

Table 1 Vibrational mode assignments of the pyridine ring in P4VP

Normal modes ^a	P4VP (cm ⁻¹)	$P4VP \cdot I_2 (cm^{-1})$	P4VP·ICl (cm ⁻¹)
8a	1597	1632/1607	1637/1610
			103//1010
8b	1556	1556	_
19a	1493	1500	1502
CH ₂ scissor	1453	1450	1452
19b	1414	1431/1423	1431
9a	1220	1213	1214/1203
12	1070	1063	1063
1	992	1023/1010	1019
11	823	830	833

^a Modes are labelled according to the Wilson notation.³⁴

A parasitic α-H substitution reaction on the polymer chain may occur due to the existence of halogen radicals in the system. Gas phase ICl is a rather unstable compound, with a formation Gibbs free energy of only -5.8 kJ mol^{-1} (303 K), and likely generates highly active Cl radicals in the gas phase.41 A fraction of the active pyridyl α-H is radically substituted and iodinated/chlorinated P4VP is formed. Hydrogen halides are formed in this process, and hence protonated pyridinium was found in the spectrum. C-Cl stretch vibration (791 cm $^{-1}$) of the chlorinated P4VP was found in the P4VP·ICl film but not in the P4VP·I₂ film (Fig. 2a), which further confirms that the α-H substitution can occur during CTC formation. In comparison, the iodine radicals generated from I2 homolysis are much less active, and hence less HI is formed in the process. 42 As a result, the intensity of the protonated pyridinium peak in the P4VP·I₂ peak is smaller than that in P4VP·ICl. It should be acknowledged that α-H substitution is not the only possible source of pyridinium in the P4VP·ICl film. ICl may react with residual moisture to form HCl, which is then absorbed by P4VP and can react further to form pyridinium which is detected by FTIR. Yet



Scheme 2 Proposed reactions between P4VP and ICI during gas phase incorporation. Thermal heterolysis of ICl may result in α -H substitution in P4VP and further generate pyridinium, which is detected by FTIR.

this reaction does not result in the formation of C-Cl, which was detected spectroscopically and electrochemically (Fig. 4), so the reaction cannot account for all of the pyridinium present in the film.

The mixed conductivity of P4VP·ICl was confirmed by measuring its conductivity using a metallized pellet. Fig. 3a shows the electrochemical impedance spectrum of the Pt|P4VP·ICl|Pt pellet. A mixed ionic-electronic conductor (MIEC) behavior, which can be roughly described as the combination of a Warburg element and an RC element (the low frequency 45° straight line is not shown in the spectrum due to the frequency limit of the instrument), was observed. The detailed fitting of MIEC impedance to resolve ionic and electronic transport, however, is complicated. 43,44 In pyridine-ICl solution, many ionic conductors such as Pv₂I⁺, Cl⁻ and ICl₂⁻ were observed, and their concentrations are linked by multiple chemical equilibria.³⁶ In the P4VP·ICl system, the relationship between ionic charge carriers is further complicated due to the existence of the polymer chain. Additionally, fitting of the MIEC impedance requires the knowledge of various microscopic properties of the material, such as the diffusion coefficient of the involved species. Yet the total conductivity can be assessed using the impedance spectrum and is presented in Fig. 3b. From 20 °C to 70 °C, the total conductivity of the P4VP·ICl film slightly decreases from 1.9×10^{-6} S cm⁻¹ to 1.7×10^{-6} S cm⁻¹. The total conductivity follows Arrhenius behavior ($r^2 = 0.99$), with a low negative activation energy $(-1.84 \text{ kJ mol}^{-1} \text{ or } -0.02)$ eV). This low negative activation energy is rarely seen in polymeric materials. The electronic conductivity of conjugated polymer semiconductors, such as polyacetylene, increases with temperature.⁵² Likewise, the ionic conductivity of polymerbased lithium ion conductors, such as PEO-Li salt mixtures, also increases with temperature. 53 However, charge transport in P4VP·ICl is not a simple combination of these two conduction mechanisms. The conductivity of the complex is directly correlated to the coordination-dissociation equilibrium of halogen in P4VP·ICl. The electrical conductivity is determined by the molecular halogen species (I₂ or ICl), as demonstrated by

the strong dependence of the electronic conductivity of P4VP·I₂ on the concentration of I2.54 On the other hand, ionic conductivity is contributed by the dissociated halogen ions (PyI+, I-, Cl⁻, ICl₂⁻ etc.), which are in equilibrium with molecular halogen and each other. These equilibria are well known in the pyridine-halogen liquid solution system.36 As a result, the temperature dependence of the conductivity of P4VP·ICl will be a strong function of the speciation of the halogens due to these multiple equilibria in the polymer film. Elucidation of the exact equilibria was beyond the scope of this project, but it is reasonable to expect that conductivity will decrease with temperature if the equilibria favor species with lower diffusivities. The electronic conductivity of P4VP|ICl was measured using chronoamperometry.45 The Pt|P4VP·ICl|Pt pellet was biased from 10 mV to 50 mV, and the stable current was found to follow Ohm's law ($r^2 = 0.9999$, Fig. 3c). From this result, P4VP·ICl appears to be semiconducting, with $\sigma_{\rm elec} = 4.14 \times 10^{-10}$ 10⁻⁷ S cm⁻¹ or 22% of the total conductivity at room temperature. The conductive nature allows us to build a relatively thick cathode. In this work, a 2.7 µm thick P4VP·ICl cathode was employed. In comparison, P4VP·I₂ only shows $\sigma_{\rm elec} = 3.6 \times$ 10⁻⁹ S cm⁻¹ at room temperature, which significantly limits the electron transport in the cathode film. It is worth noting that the conductivity of the electron donor-halogen system is governed by the amount of halogen incorporation. In this work, P4VP·I₂ and P4VP·ICl samples are vacuum dried to remove the solvent before being pressed into a pellet. As a result, the molar ratio between P4VP and halogen in the pellet is slightly >1. The measured conductivities are lower than previously reported values, which are usually measured for complexes rich in halogens, where the molar ratio of polymer: halogen is $\ll 1.46$

Since the CTC cathode is inevitably exposed to high vacuum during the LIPON deposition required for the fabrication of thin film batteries, physical stability of the CTC in a vacuum, i.e., vacuum resistance, is required for reproducible handling of the material and to achieve high discharge capacities. P4VP·ICl shows significantly higher vacuum resistance than P4VP·I2, and good reproducibility over multiple P4VP·ICl samples was

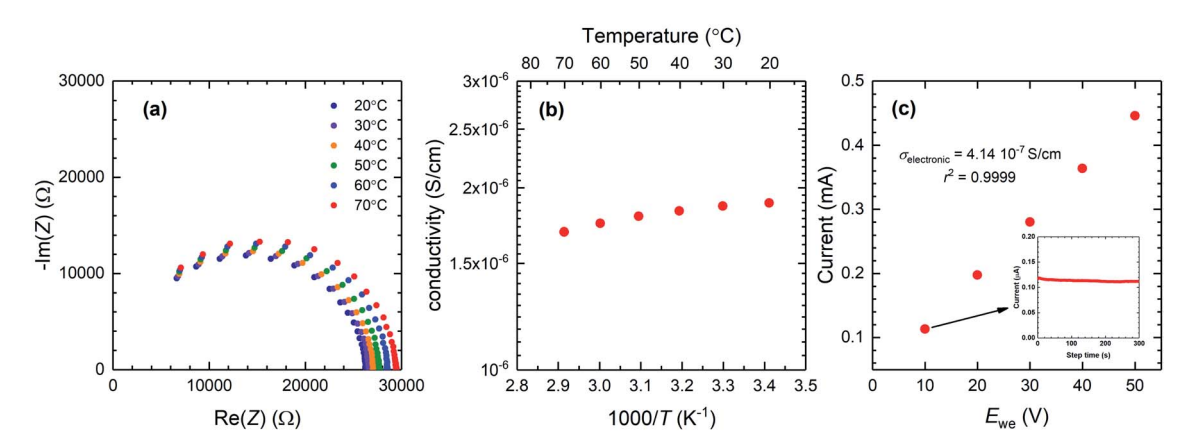


Fig. 3 Electrical characterization of P4VP·ICI. (a) EIS of the Pt|P4VP·ICI|Pt pellet; (b) total conductivity of the sample as a function of temperature; (c) I-E relationship of Pt|P4VP·ICl|Pt biased by 10 mV, 20 mV, 30 mV, 40 mV, and 50 mV at room temperature (25 °C). Inset: chronoamperogram of Pt|P4VP·ICl|Pt at 10 mV.

observed. This phenomenon can be explained by the thermodynamics of the reaction, $P4VP \cdot X_2 \rightleftharpoons P4VP + X_2$ ($X_2 = I_2$ or ICl). It was assumed that the thermodynamics are analogous to the formation of a small molecule CTC with pyridine, $Py \cdot X_2 \rightleftharpoons Py + X_2$, where the equilibrium constants are 1 \times $10^{-3} \text{ mol } L^{-1} \text{ for } Py {\cdot} I_2 \text{ and } 2 \times 10^{-6} \text{ mol } L^{-1} \text{ for } Py {\cdot} ICl \text{ at the }$ standard state.36 Hence, it is expected that the concentration of halogen molecules will be higher in P4VP·I2 than in P4VP·ICl, and they evaporate from the film during vacuum processing. Experiments revealed that P4VP·I2 lost 38% of the incorporated I₂ after 30 min of high vacuum exposure, while P4VP·ICl only lost 8% of the incorporated ICl. Another potential concern associated with the vacuum loss of halogen during LIPON deposition is the formation of a concentration gradient, which will increase the interfacial charge transfer resistance, adding to voltage losses during operation of the thin film battery. To understand this potential issue, a 2.5 µm thick P4VP·ICl film was characterized ellipsometrically before and after 30 minutes of exposure to vacuum (approx. 10^{-5} torr). The refractive index of P4VP·ICl is a function of ICl concentration with its high molar refractivity, which allows the distribution of ICl to be characterized indirectly through the development of an optical model of the film. A basic model with a single refractive index for the entire film represents an isotropic film with a uniform distribution of ICl. On the other hand, to model a gradient in ICl, the graded model divides the film into multiple layers of equal thickness and allows the refractive index to vary between each layer. Two refractive index dispersion curves were obtained, representing the refractive index of the top layer at the air-film interface and the bottom layer in contact with the substrate. The initial refractive index of the P4VP film is approximately 1.58 and increases significantly upon incorporation of ICI. Specifically, when the polymer film is modelled with a gradient index (indicative of depletion of ICl from the air-film interface), the refractive index of the top layer at 632.8 nm is 1.7449, while the bottom layer has a refractive index of 1.7578. The refractive index difference at these two interfaces is 0.0129, indicating a negligible concentration gradient from the top to bottom. Moreover, these indexes are close to the refractive index obtained using an isotropic model (1.7495), which further suggests that a negligible gradient develops. The fit quality of these two models is quantified using the mean square error (MSE), which represents the difference between the model and the experimental data. The MSE of models was optimized using a Levenberg-Marquardt regression algorithm. The minimized MSE values of the isotropic and graded model are 17.008 and 16.812, respectively, which are both reasonably small for a 2.5 µm film. The negligible difference in the MSE of 0.196 suggests that grading did not significantly improve the quality of the fit despite the additional fit parameters. Thus, it could not be concluded that a permanent concentration gradient develops upon exposure to vacuum. Given the thinness of the polymer film, equilibration of the ICl concentration within the film occurs reasonably fast - over a much shorter timescale than further processing and thin film battery operation. Owing to its higher conductivity, higher vacuum resistance and fast diffusion of ICl in P4VP matrices, P4VP·ICl was

selected as a candidate material for organic cathode thin-film batteries.

Electrochemistry of P4VP·ICl

To test the electrochemical properties of the P4VP·ICl cathode, LIPON and Li metal were deposited on the cathode to make a thin film battery. Schematic illustration of the sequential deposition is shown in Fig. S1,† and the structure of the stack is presented in Fig. 1a. Due to the low surface roughness of the cathode film, it was found that 150 nm LIPON is sufficient to completely encapsulate the cathode and reliably separate the two electrodes. A colorless LIPON layer can be seen on the uncoated part of the substrate, and the coated P4VP·ICl complex cathode maintains its slight yellow color. In comparison, the color of P4VP·I2 becomes much lighter after the deposition due to vacuum loss of I2. A Li metal anode is applied to the cathode/electrolyte stack by thermally evaporating Li metal. The anode also serves as a current collector, and no encapsulation was applied. The thin film battery is moved into another glovebox for testing.

Electrochemical reactions of the P4VP·ICl-Li system are revealed by cyclic voltammetry (Fig. 4a). The system has a stable 3.65 V open circuit voltage, which was consistent between samples and insensitive to temperature. Starting from the OCV, the system is first scanned to 2.0 V. Three peaks (3.45 V, 3.0 V, and 2.73 V vs. Li/Li⁺) can be found during the scan. The 3.45 V peak is assigned to the 1st stage reduction of ICl and the 2.73 V peak is assigned to the 2nd stage reduction of I₂:

$$2P4VP \cdot ICl + 2Li^{+} + 2e^{-} = P4VP + P4VP \cdot I_{2} + 2LiCl$$

$$E_{peak} = 3.45 \text{ V vs. Li/Li}^{+}$$
(1)

$$P4VP \cdot I_2 + 2Li^+ + 2e^- = 2LiI + P4VP$$

 $E_{peak} = 2.73 \text{ V } vs. \text{ Li/Li}^+$ (2)

Overall reaction:
$$P4VP \cdot ICl + 2Li^+ + 2e^- = LiI + LiCl + P4VP$$
(3)

The theoretical potential of the two reaction steps can be estimated using the standard formation Gibbs free energy change of ICl(s), LiCl(s) and LiI(s) (-5.7 kJ mol^{-1} , $-384.0 \text{ kJ mol}^{-1}$ and $-266.2 \text{ kJ mol}^{-1}$, respectively).⁴⁷ Without P4VP, the first step reduction of ICl has $\Delta G^{\Theta} = -756.6 \text{ kJ mol}^{-1}$, or $\varphi^{\Theta} = 3.92$ V and the second step reduction of I_2 has $\Delta G^{\Theta} =$ $-532.4 \text{ kJ mol}^{-1}$, or $\varphi^{\Theta} = 2.77 \text{ V}$. In the P4VP·ICl system, the potential of reaction (1) is also affected by the dissociation reaction of P4VP·ICl (P4VP·ICl \rightarrow P4VP + ICl, $\Delta G_1 > 0$) and the formation reaction of P4VP· I_2 (P4VP + $I_2 \rightarrow P4VP \cdot I_2$, $\Delta G_2 < 0$). Due to the stronger Lewis acidity of ICl than that of I2, free energy released by P4VP·I2 formation cannot compensate the dissociation of P4VP·ICl ($|\Delta G_1| > |\Delta G_2|$), and thus the peak potential is reduced to 3.45 V. Similarly, the potential of reaction (2) is affected by the dissociation of P4VP·I2, which reduces the peak potential from 2.77 V to 2.73 V.

The 2.73 V potential assigned to $I_2 \rightarrow LiI$ is in agreement with previous reports on electrochemistry of Li/I2.48 Thus the

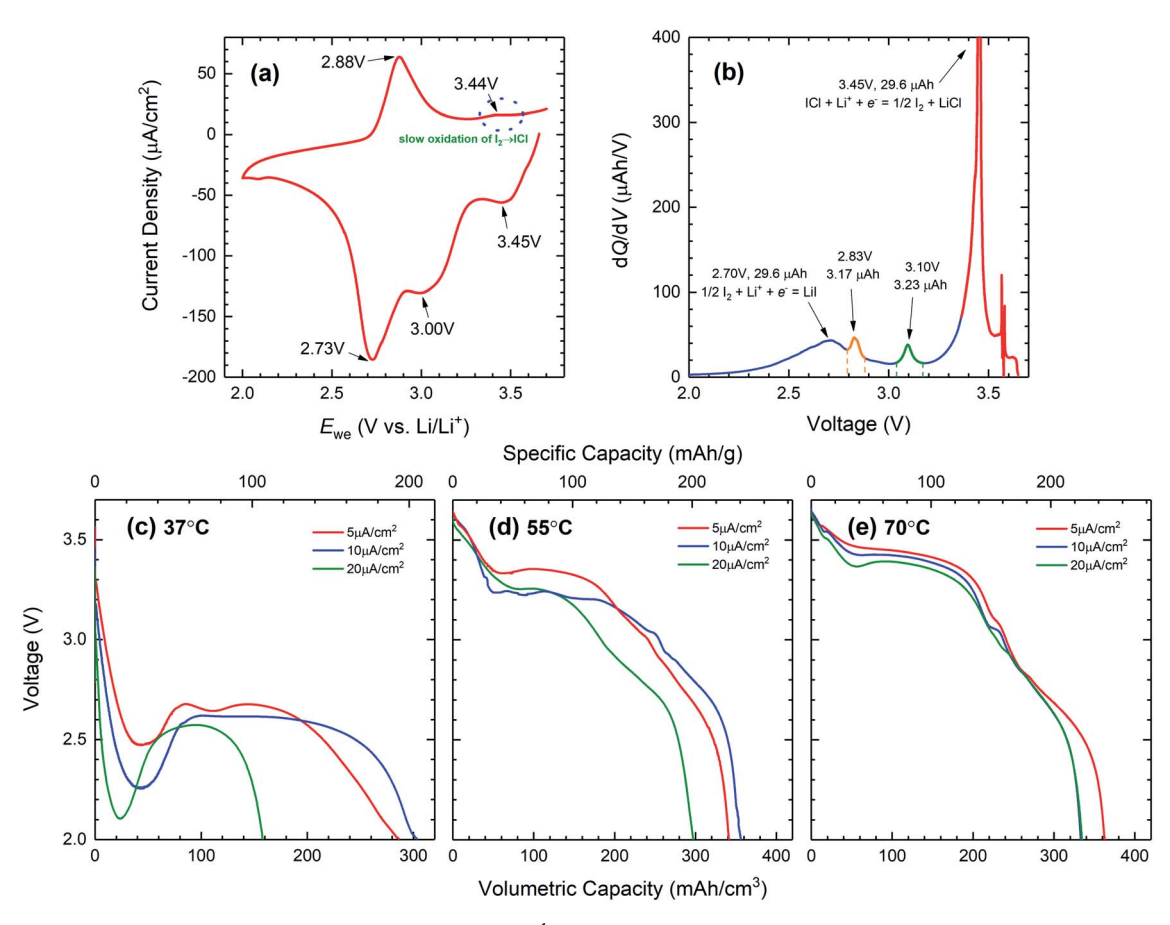


Fig. 4 (a) Cyclic voltammogram of P4VP·ICl at 70 °C and 0.5 mV s⁻¹ scan rate. (b) dQ/dV plot of 2700 nm P4VP·ICl discharge at 70 °C. (c)–(e): 1st discharge profile of a 2700 nm P4VP·ICl–LiPON–Li thin film battery. The cell was held at (c) 37 °C (d) 55 °C and (e) 70 °C. Discharge current densities of 5 μ A cm⁻², 10 μ A cm⁻² and 20 μ A cm⁻² were applied.

3.45 V and 2.73 V peaks can be attributed to eqn (1) and (2), respectively. The 2-stage reduction of P4VP·ICl is further supported by the dQ/dV plot of the 1st discharge at 70 °C (Fig. 4b). Four peaks can be found in the dQ/dV plot, with peak potentials of 3.45 V, 3.10 V, 2.83 V and 2.70 V vs. Li/Li⁺, respectively. The peak potentials of 1st stage ICl reduction and 2nd stage I2 reduction are in good agreement with CV results. An anodic scan from 2.0 V to 3.7 V vs. Li/Li⁺ was used to assess the reversibility of the system. At 2.88 V vs. Li/Li⁺, I⁻ from LiI is oxidized to I2, showing an anodic peak. However, only a small peak of I2 \rightarrow ICl is found at 3.45 V vs. Li/Li⁺, which suggests that the oxidation of I0 to I⁺ is a slow process, which will significantly restrict the recharging of the system.

Besides the reduction of P4VP·ICl and P4VP·I2, both Fig. 4a and b suggest side reactions in the system. In the cyclic voltammogram, a single peak at 3.0 V νs . Li/Li $^+$ is observed. In the dQ/dV plot, two peaks (2.83 V and 3.10 V νs . Li/Li $^+$) are found between the two major peaks. The two peaks have very similar capacity (1 : 1.01) and contribute approximately 10% of the total capacity (6.4 μ A h/59.2 μ A h). Combined with spectroscopic evidence, the two peaks are attributed to the reduction of halogen substituted P4VP (2.83 V for chlorinated P4VP and 3.10 V for iodinated P4VP). Such an attribution is indirectly

supported by the α -H substitution mechanism (Scheme 2), in which the recombination between benzyl radicals and halogen radicals should generate the two substituted compounds in a molar ratio of 1:1. In the cyclic voltammogram, the two reduction peaks cannot be distinguished, most likely due to the similar electrode kinetics and large FWHM (full width at half maximum). ⁴⁹ The 3.0 V ν s. Li/Li $^+$ peak in the voltammogram is very close to the average of the two reactions (2.97 V ν s. Li/Li $^+$), which further supports the peak assignment.

Understanding the electrochemistry of P4VP·ICl reduction allows further investigation of the P4VP·ICl|LIPON|Li thin film cell. The 1st discharge profiles of the P4VP·ICl|LiPON|Li thin film battery cells are presented in Fig. 4c–e. The cells were discharged at rates of 5 μ A cm⁻², 10 μ A cm⁻² and 20 μ A cm⁻² at 37 °C, 55 °C and 70 °C. The resulting specific capacities are summarized in Table 2. To fully discharge the cell, the discharge cut-off potential was set to 2.0 V. At 37 °C, the cell showed significant polarization, possibly due to the slow diffusion of Li⁺ in the cathode. At a 20 μ A cm⁻² current density, 1.55 V overpotential (3.65 V \rightarrow 2.10 V) was observed, which corresponds to a total cell resistance of 7.8 × 10⁴ Ω . Similarly, total cell resistances at 5 μ A cm⁻² and 10 μ A cm⁻² were 1.4 × 10⁵ Ω and 2.4 × 10⁵ Ω , respectively. The total resistance is much

Table 2 1st discharge performance of the P4VP·ICI|LIPON|Li cell

Temperature/current density	5 μA cm ⁻²	10 μA cm ⁻²	20 μA cm ⁻²
37 °C	286 mA h cm $^{-3}$ (193 mA h g $^{-1}$)	303 mA h cm $^{-3}$ (205 mA h g $^{-1}$)	158 mA h cm $^{-3}$ (107 mA h g $^{-1}$)
55 °C	341 mA h cm $^{-3}$ (230 mA h g $^{-1}$)	356 mA h cm $^{-3}$ (240 mA h g $^{-1}$)	297 mA h cm $^{-3}$ (201 mA h g $^{-1}$)
70 °C	362 mA h cm $^{-3}$ (245 mA h g $^{-1}$)	333 mA h cm $^{-3}$ (225 mA h g $^{-1}$)	335 mA h cm $^{-3}$ (226 mA h g $^{-1}$)

larger than that of the combination of the cathode and electrolyte (250 Ω for the P4VP·ICl cathode and 225 Ω for the LIPON electrolyte at 37 °C), which suggests the presence of large interfacial resistance. Such a large interfacial resistance may be related to the difference in charge carrier species of P4VP·ICl (halogen species) and LIPON (Li⁺). Similar behavior at the polymer/inorganic interface has been reported before.50 After the first 25% of the capacity, accumulation of LiCl improves the transport of Li⁺ in the cathode and a stable 2.7 V plateau is observed.

The performance is significantly improved while the cell is heated to 55 °C due to reduced cell impedance (Fig. S4†). Polarization of the cell is reduced to 400 mV, indicating significantly mitigated interfacial resistance. The cell impedance can be further reduced by heating to 70 °C, and the polarization is further reduced to <200 mV. Two distinctive voltage plateaus can be seen in the voltage profile, which correspond to the two-stage reduction of P4VP·ICl. The estimated total resistance from the cathode and electrolyte contributes <40% of the total impedance to the cell at 70 °C, suggesting that the interfacial resistance between LIPON and the P4VP·ICl cathode remains dominant. The total discharge capacity of the cell is comparable with that of layered oxide thinfilm batteries (Table 2), reaching 362 mA h cm $^{-3}$ (245 mA h g $^{-1}$). These results show that despite the presence of large interfacial resistance, P4VP·ICl allows the construction of a relatively thick cathode without a conductive additive.

Characterization of the reversibility of the P4VP·ICl cells is presented in Fig. 5 and S5.† After constant current-constant voltage (CCCV) charge of the discharged P4VP·ICl cell, considerable capacity was lost. The 2nd discharge shows that 50% of

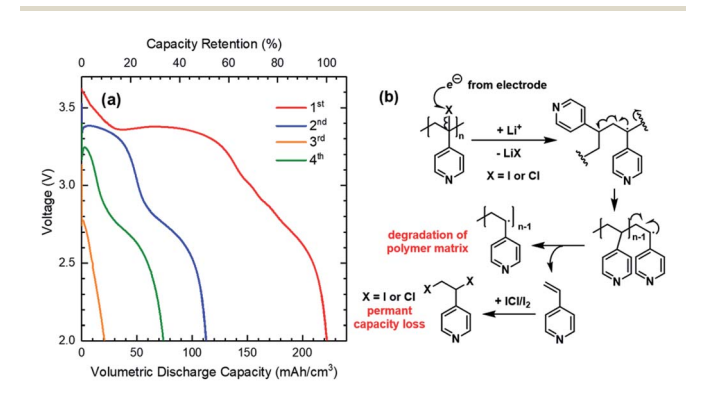


Fig. 5 (a) Discharge voltage profile of the P4VP·ICI|LIPON|Li cell. The cell was discharged at 10 μA cm⁻² to 2.0 V and recharged at 10 μA cm^{-2} to 3.7 V followed by a constant voltage step at 3.7 V at 70 °C. (b) Proposed degradation mechanism of halogen substituted P4VP.

the initial capacity is recovered. Both the \sim 3.4 V ICl \rightarrow I₂ + LiCl and the \sim 2.7 V I₂ \rightarrow LiI discharge plateaus were found in the 2nd discharge, while the initial polarization was found significantly larger than that of the 1st discharge process. As shown in Fig. 5a, the \sim 3.4 V ICl reduction plateau still appears in the 2nd and 3rd discharge cycles, despite the unsatisfactory stability of P4VP against radical substitution and fast consumption of the active material. The 2.7 V I2 reduction plateau is also found in the 4th discharge cycle, while the ICl reduction plateau disappeared. This evidence suggests that the conversion of LiI to I2 is easier than the conversion of I2 and LiCl to ICl. Similar observation was made in the cyclic voltammogram (Fig. 4a), which shows that the kinetics of I⁰ oxidation to I⁺ is much slower than that of I^- to I^0 . It is possible that the I^0 or Cl^0 radical intermediates during charge can also react with α-H of the polymer backbone to form iodinated/chlorinated P4VP, which will result in further capacity loss. Thus, it is expected that the α -H bearing P4VP·ICl system may have poor recharge behavior.

Voltage profiles of the charge steps are included in Fig. S5.† Significant charge capacity decay was observed in the first 4 cycles. An increase of the polarization of the cell was found during charge, indicating increased cell impedance due to the degradation of the polymer matrix and depletion of the active material. A notable phenomenon was observed, where the overpotential decreases during the galvanostatic charge. Such behavior can be explained by varying cathode conductivity during charge. Since the electronic conductivity of the complex is directly related to the concentration of halogen (I2 or ICl) complexed to the polymer matrix, cathode electronic conductivity is expected to increase as more X2 forms during the anodic reaction, resulting in less polarization. Initially during recharge, the cell potential is mainly determined by polarization, but as the charge progresses and conductivity increases, the polarization will decrease and the charge potentials more closely approach the equilibrium potential of the P4VP·X2 complex. As a result of the polymer matrix degradation, active material depletion and increasing polarization, the conversion of I2 to ICl is increasingly inhibited over increased cycle number. The voltage plateau at 3.4 V associated with ICl formation is completely absent in the voltage profiles by the 4th discharge, further revealing the limited reversibility of this system. The reduction of iodinated/chlorinated P4VP may follow the proposed mechanism in Fig. 5b, resulting in molecular weight reduction and impedance increase. Similar to the electrochemical reduction of other halogenated hydrocarbons, degradation of the P4VP matrix starts with the formation of benzyl radicals at the halogenated site.51 The benzyl radicals will cause chain severance and depolymerization of P4VP. The released 4VP monomer will further react with ICl/I2 generated from the oxidation of LiCl/LiI and reduce the discharge capacity. The overall effect is a significant decrease in molecular weight and consumption of the active material. Due to the low sample mass and strong interaction between P4VP and ICl, experimental confirmation of the P4VP molecular weight after discharge was not possible. Although significant capacity fading is observed during the recharge, it is expected that the cyclability of a polymeric charge transfer complex cathode can be significantly improved if the halogenation reaction during ICl incorporation is prevented. Since the halogenation reaction is directly related to the activity of α-H in the P4VP structure, replacing the α-H with a less reactive moiety, such as a methyl or nitrile group, should significantly improve the stability of the polymer during the halogen incorporation process and the recharge process.

Flexible battery enabled by P4VP·ICl

Due to the advantage of the iCVD technique and P4VP·ICl gas phase incorporation chemistry, the battery can be made flexible by simply replacing conventional rigid inorganic substrates with flexible plastics without additional processing. Fig. 6 shows the performance of a flexible P4VP·ICl battery on a polyimide (Kapton) substrate. The battery can be bent 180° without compromising its electrochemical performance (discharge capacity was 328 mA h cm⁻³). The discharge profile of the cell shows two distinctive discharge reactions, as demonstrated in cells fabricated on quartz substrates. This evidence suggests that an iCVD-deposited, organic cathode can achieve true flexibility without any additional processing, while previous flexible battery systems, including liquid, solid-state and thin-film batteries require complete redesign of the cell. Thus,

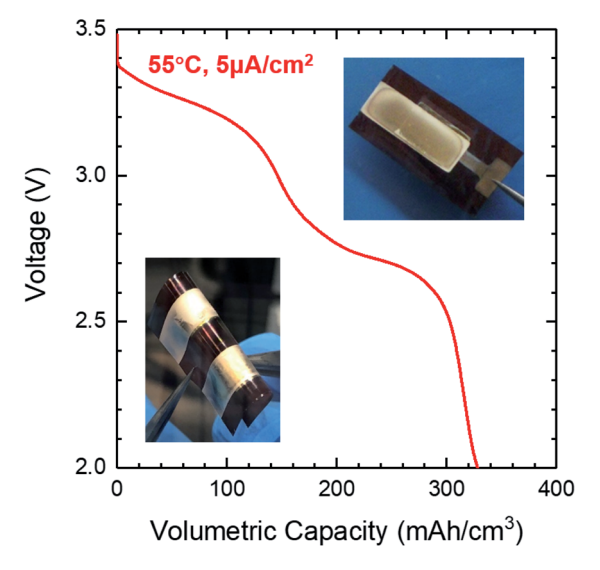


Fig. 6 Discharge profile of the flexible P4VP·ICl|LIPON|Li cell coated on a Kapton® film after bending. Cell temperature was 55 °C, and current density was 5 μ A cm $^{-2}$. Bottom inset: picture of flexible thin film batteries (two batteries were deposited on this substrate). Top inset: plan view of the battery before cycling.

a polymeric charge transfer complex cathode has considerable potential for application in advanced Li-ion batteries.

Conclusions

P4VP·ICl charge transfer complexes have been demonstrated as polymeric, readily processable cathodes for solid state lithium thin-film batteries. Smooth P4VP thin films were prepared with iCVD, and then further incorporated with ICl and I2 to form 1:1 charge transfer complexes. With EIS and chronoamperometry, P4VP·ICl was confirmed to be both ionically and electronically conductive, with a total conductivity of $1.7 \times 10^{-6} \text{ S cm}^{-1}$ and electronic conductivity of 4.1×10^{-7} S cm⁻¹ at room temperature. The improved transport phenomenon enabled the construction of a smooth, uniform 2.7 µm-thick cathode, where only 150 nm LIPON electrolyte was needed to fully encapsulate the cathode. At elevated temperature, the P4VP·ICl|LIPON|Li cell can deliver 245 mA h g⁻¹ specific capacity and a voltage of 3.65 V. To the best of our knowledge, this is the first demonstration of polymer charge transfer complexes in thin-film batteries. The system showed considerable interfacial resistance, presumably due to the difference in charge carriers at the P4VP·ICl and LIPON interface. Detailed spectroscopic and electrochemical characterization of the cathode suggested that the electrochemical reaction ICl + 2Li → LiI + LiCl is partially reversible in P4VP matrices; its reversibility is mainly limited by the poor chemical stability of P4VP due to the presence of an active hydrogen. Eliminating the active α-H from the polymer structure should greatly improve the stability of the polymer matrices. iCVD polymerization of α-substituted 4-vinylpyridine derivatives should result in polymeric materials resistant to halogenation by ICl or I2, while retaining the desirable properties of charge transfer complex cathodes including sustainability, simple processing, and flexibility. The investigation of these novel polymer chemistries for thin film CTC cathodes is expected to be an important direction for continued research.

Conflicts of interest

The authors declare no conflict of interest.

Acknowledgements

This study is supported by the National Science Foundation under Grant No. CBET-1845805 and CBET-1827904 (ellipsometer).

References

- 1 J. F. M. Oudenhoven, R. J. M. Vullers and R. Schaijk, *Int. J. Energy Res.*, 2012, **36**, 1139–1150.
- 2 A. Patil, V. Patil, D. Wook Shin, J.-W. Choi, D.-S. Paik and S.-J. Yoon, *Mater. Res. Bull.*, 2008, **43**, 1913–1942.
- 3 M. E. Donders, W. M. Arnoldbik, H. C. M. Knoops, W. M. M. Kessels and P. H. L. Notten, *J. Electrochem. Soc.*, 2013, **160**, A3066–A3071.

- 4 S. Lobe, A. Bauer, S. Uhlenbruck and D. Fattakhova-Rohlfing, Adv. Sci., 2021, 2002044, DOI: 10.1002/advs.202002044.
- 5 Y. Su, J. Falgenhauer, A. Polity, T. Leichtweiß, A. Kronenberger, J. Obel, S. Zhou, D. Schlettwein, J. Janek and B. K. Meyer, Solid State Ionics, 2015, 282, 63-69.
- 6 E. G. Herbert, W. E. Tenhaeff, N. J. Dudney and G. M. Pharr, Thin Solid Films, 2011, 520, 413-418.
- 7 M. S. J. Hashmi, Comprehensive Materials Processing, Elsevier, 2014.
- 8 M. Koo, K. I. Park, S. H. Lee, M. Suh, D. Y. Jeon, J. W. Choi, K. Kang and K. J. Lee, Nano Lett., 2012, 12, 4810-4816.
- 9 J. B. Bates, N. J. Dudney, B. J. Neudecker, F. X. Hart, H. P. Jun and S. A. Hackney, J. Electrochem. Soc., 2000, 147, 59-70.
- 10 X. Zhao, Z. Zhao-Karger, M. Fichtner and X. Shen, Angew. Chem., Int. Ed. Engl., 2020, 59, 5902-5949.
- 11 J. B. Goodenough and K. S. Park, J. Am. Chem. Soc., 2013, 135, 1167-1176.
- 12 J. Heiska, M. Nisula and M. Karppinen, J. Mater. Chem. A, 2019, 7, 18735-18758.
- 13 J. J. Shea and C. Luo, ACS Appl. Mater. Interfaces, 2020, 12, 5361-5380.
- 14 M. Nisula and M. Karppinen, J. Mater. Chem. A, 2018, 6, 7027-7033.
- 15 Y.-N. Zhou, M.-Z. Xue and Z.-W. Fu, J. Power Sources, 2013, 234, 310-332.
- 16 K. K. Gleason and P. Baumann, CVD Polymers: Fabrication of Organic Surfaces and Devices. Wiley-VCH, Weinheim, Germany, 2015.
- 17 A. Asatekin, M. C. Barr, H. Baxamusa, K. K. S. Lau, W. E. Tenhaeff, J. P. Xu and K. K. Gleason, Mater. Today, 2010, 13, 26-33.
- 18 S. Aronson, P. Epstein, D. B. Aronson and G. Wieder, J. Phys. Chem., 1982, 86, 1035-1037.
- 19 W. Greatbatch, R. Mead and F. Rudolph, U.S. Pat. 3957533,
- 20 Z. Meng, H. Tian, S. Zhang, X. Yan, H. Ying, W. He, C. Liang, W. Zhang, X. Hou and W. Q. Han, ACS Appl. Mater. Interfaces, 2018, 10, 17933-17941.
- 21 Y. Zhao, L. Wang and H. R. Byon, Nat. Commun., 2013, 4,
- 22 Y. L. Wang, Q. L. Sun, Q. Q. Zhao, J. S. Cao and S. H. Ye, Energy Environ. Sci., 2011, 4, 3947.
- 23 F.-C. Liu, W.-M. Liu, M.-H. Zhan, Z.-W. Fu and H. Li, Energy Environ. Sci., 2011, 4, 1261.
- 24 A. Gero and J. J. Markham, J. Org. Chem., 1951, 16, 1835-1838.
- 25 W. E. Tenhaeff, L. D. McIntosh and K. K. Gleason, Adv. Funct. Mater., 2010, 20, 1144-1151.
- 26 B. B. Peterson, E. M. Andrews, F. Hung and J. C. Flake, J. Power Sources, 2021, 492, 229658.
- 27 Y. Zhao, N. Huo, S. Ye, A. Boromand, A. J. Ouderkirk and W. E. Tenhaeff, Adv. Opt. Mater., 2021, 2100334, DOI: 10.1002/adom.202100334.
- 28 H. Xia and L. Lu, Electrochim. Acta, 2007, 52, 7014-7021.

- 29 C. M. Julien, A. Mauger and O. M. Hussain, Materials, 2019, 12, 2687.
- 30 F. Fairbrother, Nature, 1947, 160, 87.
- 31 M. I. Bernal-Uruchurtu, G. Kerenskaya and K. C. Janda, Int. Rev. Phys. Chem., 2009, 28, 223-265.
- 32 G. Cavallo, P. Metrangolo, R. Milani, T. Pilati, A. Priimagi, G. Resnati and G. Terraneo, Chem. Rev., 2016, 116, 2478-2601.
- 33 W. B. Person, R. E. Humphrey, W. A. Deskin and A. I. Popov, J. Am. Chem. Soc., 1958, 80, 2049-2053.
- 34 E. B. Wilson, Phys. Rev., 1934, 45, 706-714.
- 35 E. Groppo, M. J. Uddin, O. Zavorotynska, A. Damin, J. G. Vitillo, G. Spoto and A. Zecchina, J. Phys. Chem. C, 2008, 112, 19493-19500.
- 36 A. I. Popov and R. H. Rygg, J. Am. Chem. Soc., 1957, 79, 4622-4625.
- 37 E. W. William, director, NIST Chemistry WebBook, NIST Standard Reference Database Number 69, ed. P.J. Linstrom and W.G. Mallard, National Institute of Standards and Technology, Gaithersburg MD, p. 20899, DOI: 10.18434/ T4D303, (retrieved July 28, 2021).
- 38 B. Golec, P. Das, M. Bahou and Y. P. Lee, J. Phys. Chem. A, 2013, 117, 13680-13690.
- 39 D. Cook, Can. J. Chem., 1961, 30, 2009-2024.
- 40 A. J. Coury and P. T. Cahalan, J. Electrochem. Soc., 1980, 127, 2119-2122.
- 41 M. W. Chase, J. Phys. Chem. Ref. Data, 1998, Monograph 9, 1-1951.
- 42 G. Patrick, Organic Chemistry, Garland Science, 2012.
- 43 J. Jamnik and J. Maier, J. Electrochem. Soc., 1999, 146, 4183-
- 44 W. Lai and S. M. Haile, J. Am. Ceram. Soc., 2005, 88, 2979-2997.
- 45 W. Yourey, L. Weinstein and G. G. Amatucci, Solid State Ionics, 2011, 204-205, 80-86.
- 46 S. Moulay, J. Polym. Eng., 2013, 33, 389-443.
- 47 D. R. Burgass, P. J. Linstrom and W. G. Mallard, NIST Chemistry WebBook, NIST standard reference database number 69.
- 48 M. Xing, Z. Z. Zhao, Y. J. Zhang, J. W. Zhao, G. L. Cui and J. H. Dai, Mater. Today Energy, 2020, 18, 100534.
- 49 A. J. Bard and L. R. Faulkner, Electrochemical Methods: Fundmentals and Applications, John Wiley and Sons, 2001.
- 50 W. E. Tenhaeff, X. Yu, K. Hong, K. A. Perry and N. J. Dudney, J. Electrochem. Soc., 2011, 158, A1143-A1149.
- 51 M. Yan, Y. Kawamata and P. S. Baran, Chem. Rev., 2017, 117, 13230-13319.
- 52 N. Basescu, Z.-X. Liu, D. Moses, A. J. Heeger, H. Naarmann and N. Theophilou, *Nature*, 1987, 327, 403-405.
- 53 D. T. Hallinan and N. P. Balsara, Annu. Rev. Mater. Res., 2013, 43, 503-525.
- 54 S. Aronson, S. Wilensky, K. Jawitz and H. Teoh, Polymer, 1986, 27, 101-104.